Single-layer intrinsic 2H-phase LuX_2 (X = Cl, Br, I) with large valley polarization and anomalous valley Hall effect

Chun-Sheng Hu(胡春生), Yun-Jing Wu(仵允京), Yuan-Shuo Liu(刘元硕), Shuai Fu(傅帅), Xiao-Ning Cui(崔晓宁), Yi-Hao Wang(王易昊), and Chang-Wen Zhang(张昌文)[†]

School of Physics and Technology, University of Jinan, Jinan 250022, *China*

(Received 4 June 2022; revised manuscript received 14 August 2022; accepted manuscript online 16 August 2022)

Manipulation of the valley degree of freedom provides a new path for quantum information technology, but the real intrinsic large valley-polarization materials are rarely reported up to date. Here, we perform first-principles calculations to predict a class of 2H-phase single layer (SL) materials LuX_2 (X = Cl, Br, I) to be ideal candidates. SL-LuX_2 are ferrovalley materials with a giant valley-polarization of 55 meV–148 meV as a result of its large spin–orbital coupling (SOC) and intrinsic ferromagnetism (FM). The magnetic transition temperatures of SL-LuI_2 and SL-LuCl_2 are estimated to be 89 K–124 K, with a sizable magnetic anisotropy at out-of-plane direction. Remarkably, the anomalous valley Hall effect (AVHE) can be controlled in SL-LuX_2 when an external electric field is applied. Moreover, the intrinsic valley-polarization of SL-LuI_2 is highly robust for biaxial strain. These findings provide a promising ferrovalley material system for the experimentation of valleytronics and subsequent applications.

Keywords: intrinsic ferrovalley, anomalous valley Hall effect, first-principles calculations

PACS: 73.43.–f, 71.20.–b, 73.90.+f, 71.15.Dx **DOI:** 10.1088/1674-1056/ac89d6

1. Introduction

Valleytronics, aims at encoding, transferring, and storing information by using the valley degree of freedom, which is characterized by a local energy extreme in the band. Like the actual spin degree of freedom, the valley index is a good quantum number, which is robust against the scatterings of smooth deformations and phonons. So, the higher storage density and energy saving make these valley materials charming for the next generation of information technology. It is worth noting that the interesting phenomenon of anomalous valley Hall effect (AVHE) based on valley degrees of freedom has been extensively researched in two-dimensional (2D) hexagonal materials.[1–3] For better application, valley materials may have a large valley polarization at the unequal k point of the momentum space, that is, the valley of the two k points has a large energy difference, so that the electrons can better resist phonons and smooth deformation scattering, as if traveling through the highway. Therefore, the important principle in realizing applications is inducing large valley polarization, which not only selectively generates or manipulates carriers in different valleys, but also minimizes the effects of thermal noise in valley electronic devices.

Normally, external tunings including the optical pumping,[1,4] the magnetic doping,[5,6] the magnetic proximity effect,[7–10] or magnetic field,[11,12] etc. are essential. It is obviously inconvenient to realize a valley polarization device by using an optical pump with complex equipment.[1,4] For 2D transition metal dichalcogenides (TMDs) thin films, magnetic doping forms surface clusters that increase scattering during transmission. Moreover, the performance of the main material is inevitably affected by the magnetic substrate and increases the energy loss.[7–10] Last but not least, 1 T magnetic field can only induce 0.1 meV–0.2 meV valley polarization.[11,12] Therefore, finding valley polarization that does not require external induction is urgent. Fortunately, recent studies of 2D ferrovalley materials have shown that they have intrinsic valley polarization, which undoubtedly opens up a new path for the practical application of valley polarization. With the breaking of the time-reversal symmetry (T), space-reversal symmetry (P), and large spin–orbital coupling (SOC), 2D ferrovalley materials successfully achieved spontaneous valley polarization without external induction. So far, however, few discoveries of this material have been made, i.e., H-VSe_2,[13,14] H-$FeCl_2$,[15] MnPX_3 (X = S, Se),[16] LaBrY (Y = Br, I),[17,18] and VSi_2N_4.[19] While there are also some flaws in these discovered materials: the theoretical prediction for VSe_2 is the H phase, but experimental results show that it is the T phase, and its magnetic state is still debatable;[20–22] H-$FeCl_2$ is a hexagonal structure but does not exist experimentally;[15] as for the spontaneous valley polarization of the presence of other materials, it is very small (15 meV–63 meV).[16,17,19] Only a few can be more than 100 meV, like GdI_2.[23] However, the magnetic anisotropy energy (MAE) of GdI_2 is in plane.[24] This means that the spin orientations of Gd atoms can be random, and it is difficult to realize the long-range magnetic ordering without an external field.[25] In order to facilitate experimental exploration and then achieve applications, it is urgent to find new 2D ferromagnetic semiconductors with greater spontaneous valley polarization.

[†]Corresponding author. E-mail: ss_zhangchw@ujn.edu.cn

© 2023 Chinese Physical Society and IOP Publishing Ltd

We found that SL-LuX_2 and 2H-MoS_2 are isostructural, so similar inversion symmetry breaking and K-valley in 2H-MoS_2 appear in SL-LuX_2. Lu's strong SOC will create a large split between the two valleys, as Lu is a heavy rare earth element with a d electron. What is more, the MAE of LuI_2 and $LuCl_2$ are out of plane. Given the above properties, SL-LuX_2 is expected to be ferromagnetic semiconducting materials with large spontaneous valley splitting. In this work, large spontaneous valley splitting in SL-LuX_2 is revealed through first-principles simulations through their band structures including the SOC effect. Through calculations such as the Berry curvature, we also confirm that AVHE can be implemented in these materials. It was also found that applying a biaxial tensile strain in SL-LuI_2 can further enhance valley polarization. Therefore, SL-LuX_2 is an intrinsic ferrovalley material with great application prospects in valleytronics.

2. Computational details

The first-principles calculations are performed by using the projector augmented-wave[26,27] method as implemented in the Vienna *ab initio* simulation package (VASP).[28,29] Dealing with the exchange–correlation interaction of different electrons, we used the Perdew–Burke–Ernzerhof (PBE)[30] type generalized gradient approximation (GGA).[31] The cutoff energy is 400 eV. $9\times9\times1$ k grids for structural relaxation were used in the Brillouin-zone convergence center. Force and energy convergence accuracies are 0.01 eV/Å and 10^{-6} eV/atom, respectively. To avoid interaction between adjacent layers, we set up a vacuum space of 25 Å. The GGA+U method[32] is adopted. 3.0 eV is set to the Hubbard-U parameter. SOC[33] is used for related calculations. The phonon dispersion is obtained by the PHONOPY code[34] based on the density functional theory (DFT)[35] using a $4\times4\times1$ supercell. *Ab initio* molecular dynamic (AIMD)[36] simulation is run[37,38] at 300 K with a $3\times3\times1$ supercell. The WANNIER90 package[39] is used to calculate anomalous Hall conductivity and the Berry curvature.

3. Results and discussion

3.1. Structural properties and stability of SL-LuX_2

The lattice constants of SL-LuX_2 are shown in Table 1. Like monolayer GdI_2,[23] SL-LuX_2 are ferrovalley materials, whose crystal structures are demonstrated in Fig. 1(a). From the side view on Fig. 1(a) we can clearly see that the two layers of X atoms and the middle layer of Lu atoms form a sandwich-like unit cell. The Lu atoms in the middle layer coordinate with the six nearest neighboring X atoms to form a triangular prism. As shown in the ELF of Fig. 1(b), the Lu and I atoms are ion-bonded because electrons are mostly located near the I atoms, with no electron aggregation in between. That is, in the SL-LuX_2 structure, Lu donates two of its electrons to two X atoms, respectively, and Lu^{2+} and X^- ions are formed. In contrast, there is a large number of electron aggregations in the middle of Lu atoms in the same layer, which reduces the positive electrical repulsion between the two nuclei, so that the energy of the system is reduced, forming a stable structure, so SL-LuX_2 are transition crystals with both ionic bonds and covalent bonds. This similar feature is also found in $LaBr_2$.[17] Taking LuI_2 as an example, we calculated its molecular dynamics and phonon dispersion spectra, which are shown in Figs. 1(c) and 1(d), respectively. The small energy fluctuations and the preservation of structural integrity revealed by AIMD, as well as the phonon spectrum without imaginary frequency, prove that the SL-LuX_2 structure has good thermodynamic stability.

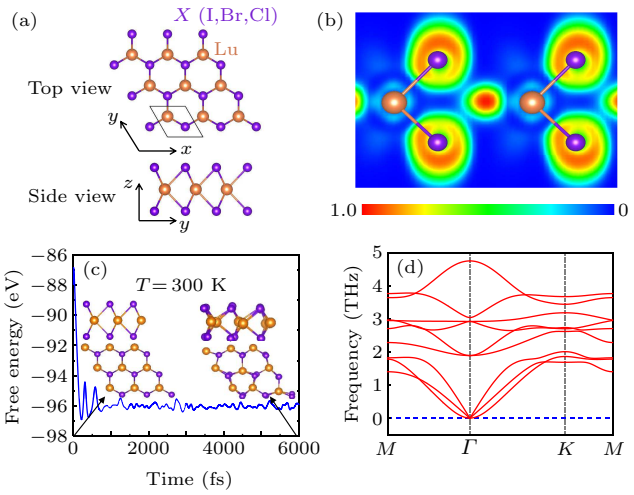


Fig. 1. Geometry and stability of SL-LuX_2. (a) Top and side views of SL-LuX_2. The box denotes the unit cell. (b) electron localization function (ELF) of SL-LuI_2. (c) Molecular dynamics simulation of SL-LuI_2 at 300 K. (d) Phonon dispersion spectrum of SL-LuI_2.

It is known that $5d^16s^2$ is the electronic configuration of Lu, so the theoretical magnetic moment of about 1.0 μ_B/Lu is the result of the 5d and 6s shells. We compared the FM and antiferromagnetic (AFM) states of the $2\times2\times1$ supercell. The results show that SL-LuX_2 are a class of ferromagnetic materials. Because for SL-LuX_2, the energy of the FM state is 11 meV/Lu, 17 meV/Lu, and 15 meV/Lu lower than the AFM state, respectively. Furthermore, considering that SL-LuX_2 have band gaps of 0.301 eV–0.681 eV (see Table 1), so SL-LuX_2 are 2D FM semiconductors. To date, only a few 2D materials with FM intrinsic semiconductor properties have been found experimentally, such as SL CrI_3[40] and $Cr_2Ge_2Te_6$.[41] The intrinsic FM semiconductors, SL-LuX_2 combined with their stability would make them very promising for experimental explorations. What is more, SL-LuX_2 are also bipolar-magnetic semiconductors. As is shown in Figs. 3(c) and 4, the conduction band-minimum (CBM) and valence band-maximum (VBM) of SL-LuX_2 are mostly by different spin states contributed. And similar results were found in $LaBr_2$[17] and GdI_2.[23] So, SL-LuX_2 can easily be shifted

into a half-metal with tunable spin-polarization by carrier doping.

Table 1. The lattice parameters of SL-LuX_2: $l_{X-\mathrm{Lu}}$, d_{XX}, and $\angle X\mathrm{Lu}X$, represent the bond length of X and Lu atoms, the distance between two X atoms, and bond angle of Lu and the two X atoms, respectively. We computed formation energy, and band gaps without SOC and with SOC and E_{for}, $E_{\mathrm{g\text{-}PBE}}$, $E_{\mathrm{g\text{-}PBE+SOC}}$. E_{FM} (E_{AFM}) is the energy of FM (AFM) state. T_{c} is Curie temperature, while T_{BKT} is the critical temperature of Berezinskii–Kosterlitz–Thouless (BKT) transition.

	LuI_2	$LuBr_2$	$LuCl_2$
$a = b$ (Å)	4.06	3.83	3.71
$l_{X-\mathrm{Lu}}$(Å)	3.122	2.910	2.757
d_{XX} (Å)	2.029	1.915	1.853
$\angle X\mathrm{Lu}X$ (°)	81.10	82.29	84.47
E_{for} (eV/atom)	−2.672	−3.229	−3.715
$E_{\mathrm{g\text{-}PBE}}$ (eV)	0.301	0.554	0.618
$E_{\mathrm{g\text{-}PBE+SOC}}$ (eV)	0.212	0.486	0.687
E_{FM} (eV)	−38.957471	−45.103244	−50.622901
E_{AFM} (eV)	−38.913845	−45.042369	−50.555515
J (meV)	5.45325		8.42325
D (meV)	−3.64		−0.21
$T_{\mathrm{c/BKT}}$ (K)	124	78 (T_{BKT})	89

If E_{tot} and $E_{X/\mathrm{Lu}}$ are used to represent the total ground state energy of the SL-LuX_2 unit cell and the energy of the X or Lu atom alone, then its formation energy can be obtained by the following formula:

$$E_{\mathrm{for}} = [E_{\mathrm{tot}} - (2E_X + E_{\mathrm{Lu}})]/3.$$

As shown in Table 1, the formation energy of SL-LuX_2 is all negative, implying that they are easy to form in terms of energy.

Furthermore, we calculate the Curie temperature (T_{c}) of SL-LuI_2 and SL-$LuCl_2$ by the Heisenberg model. And from the spin configuration of Fig. 2(a), the energies of the FM state and the AFM state can be obtained as follows:

$$E_{\mathrm{FM}} = E_0 - 6JS^2,$$
$$E_{\mathrm{AFM}} = E_0 + 2JS^2,$$

where E_0 is the total energy excluding the magnetic coupling. And J (the exchange parameters of the nearest-neighbor) can be obtained by $J = (E_{\mathrm{AFM}} - E_{\mathrm{FM}})/8S^2$, where S is the total magnetic moment of the single unit cell, which is $1\mu_{\mathrm{B}}$. Taking into account magnetic anisotropy, we calculated the magnetic crystal anisotropy coefficient D. We estimate the D value with MAE/S^2. J and D values are shown in Table 1. We used mcsolver[42] to do the Monte Carlo simulations and got the T_{c} as shown in the Fig. 2(b).

As for SL-$LuBr_2$, its magnetic anisotropy (MAE) is in-plane. The Mermin–Wagner theorem[43] prohibits ferromagnetic order in 2D materials that have continuous spin symmetries. This means that 2D materials with an easy magnetization plane do not exhibit a ferromagnetic phase transition, but instead, a Berezinskii–Kosterlitz–Thouless (BKT) transition to a quasi-long-range ordered low-temperature phase with a power-law decay of the correlation function.[44] The BKT transition of SL-$LuBr_2$ could occur at the critical temperature T_{BKT}, which can be calculated as $T_{\mathrm{BKT}} = 0.89\ (E_{\mathrm{AFM}} - E_{\mathrm{FM}})/8k_{\mathrm{B}}$,[45,46] where k_{B} is the Boltzmann constant. Therefore, from the $E_{\mathrm{AFM/FM}}$ in Table 1, we can calculate that the T_{BKT} of SL-$LuBr_2$ is about 78 K, which is very close to the temperature of liquid nitrogen.

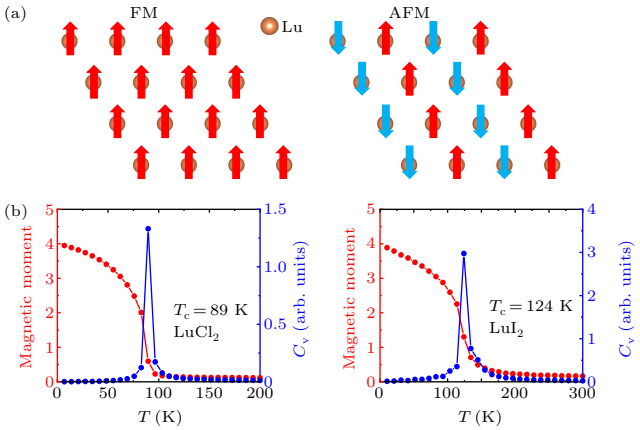


Fig. 2. (a) The magnetic configuration of FM and AFM. The up (down) magnetic moments are represented by red (bule) arrows. (b) The coordinate axes on the left and right sides indicate the magnetic moment and heat capacity, respectively. Red and blue dot lines indicate the magnetic moment and specific heat of LuX_2 varying with temperature, respectively.

3.2. Spin and valley polarization of SL-LuX_2

The band structures of SL-LuX_2 are shown in Figs. 3(a) and 4, respectively. We can find that they have a pair of degenerate energy extreme located at the high symmetry points of K and K' in the valence and conduction bands. Therefore, SL-LuX_2 become the valley materials. And unlike ordinary valley-polarized materials, SL-LuX_2 are bipolar magnetic semiconductors because of its nearly fully spin-polarized valence and conduction bands in opposite spin channels. After considering SOC, as shown in Figs. 3(b) and 4, the spin degeneracy of the bands is broken. Not only the degenerate of the valence bands, but also the conduction bands are breaking at the same time. As a result, the valley polarizations up to 55 meV, 93 meV, and 148 meV, respectively, are generated in SL-LuX_2 [see Figs. 3(b) and 4], which corresponds to the result that an externally induced magnetic field of up to 745 T–1490 T is applied.

To determine the magnetic anisotropy energy (MAE) of SL-LuX_2, we calculate the energy in the direction of the three spin axes of Lu atoms when the SOC effect is considered. That is, E_{100} (x-axis) and E_{010} (y-axis) in the plane, E_{001} (z-axis) outside the plane. Because E_{100} and E_{010} are almost the same, we define MAE $= E_{001} - \min\{E_{100}, E_{010}\}$, which are −3.64 meV, 0.08 meV, and −0.21 meV for LuI_2, $LuBr_2$, and $LuCl_2$, respectively. For SL-$LuBr_2$, the MAE is much smaller than 1 meV, which can be easily modulated by magnetic fields. As for SL-LuI_2 and SL-$LuCl_2$, their MAE are rarely negative in 2D valley-polarization materials, which demonstrate that the easy axis is out of plane. So, unlike Ni_3I_8[47]

and VSi_2N_4,[19] SL-LuI_2 and SL $LuCl_2$ can realize valley-polarization without magnetic substrates.

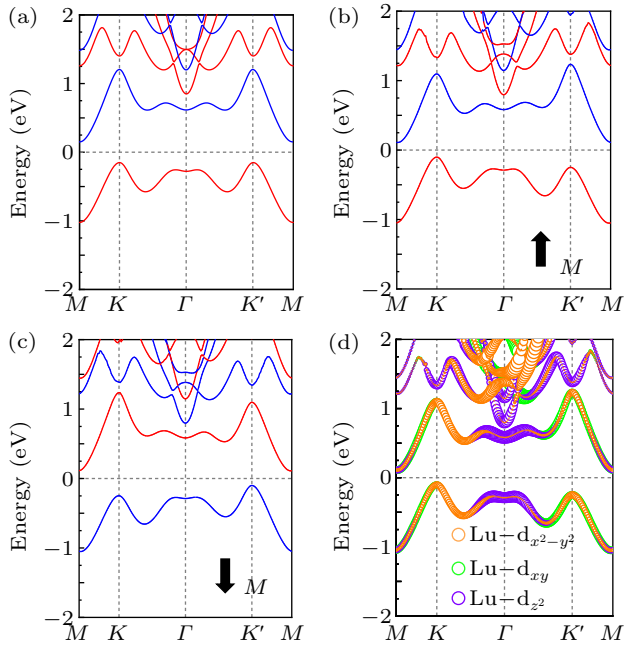


Fig. 3. Band structure of SL-LuI_2. (a) SOC is not considered; (b) and (c) SOC is considered, but the magnetic moment of the Lu atom is reversed; (d) orbital-projected band structure of SL-LuI_2. Spin up and down are shown in red and blue, respectively.

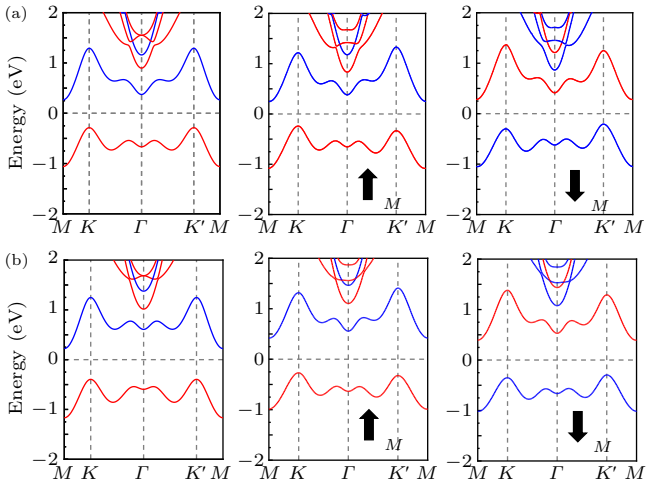


Fig. 4. The band structure of LuX_2 (X = Br, Cl), and the two figures on the far left do not consider SOC. (a) $LuBr_2$, (b) $LuCl_2$.

In order to analyze the source of valley polarization of SL-LuX_2 from the atomic orbital level. Taking SL-LuI_2 as an example, we calculated and plotted orbital-projected band structure shown in Fig. 3(d). It can be seen that the Lu-d$_{x^2-y^2}$ and Lu-d$_{xy}$ orbitals are the main contributions of the valley states at K and K'. Furthermore, the Lu-d$_{x^2-y^2}$ and Lu-d$_{xy}$ orbitals degenerate and hybridize with the Lu-d$_{z^2}$ orbital, and Lu-d$_{z^2}$ is dominant near the Γ point. 2H-MoS_2 also has similar orbital distributions.[48] And because it has been proved above, SL-LuX_2 are semiconductors with intrinsic FM. Therefore, the sizeable spontaneous valley polarization in SL-LuX_2 originates from the magnetic exchange interaction of Lu-d electrons combined with SOC.

3.3. Valley Hall effect in SL-LuX_2

The Berry curvature is obtained on the basis of the Kudo formula, which can be written as

$$\Omega = -\sum_{n}\sum_{n\neq n'} f_n \frac{2\mathrm{Im}\langle\psi_{nk}|v_y|\psi_{n'k}\rangle\langle\psi_{n'k}|v_y|\psi_{nk}\rangle}{(E_n - E_{n'})^2}.$$

Here, the band indexes are n and n', and f_n is the Fermi–Dirac distribution function, and $\psi_{nk/n'k}$ is the Bloch wave function with eigenvalue $E_{n/n'}$, and $v_{x/y}$ is the velocity operator along x/y directions.

As shown in Figs. 5(a), 5(b), and 6, the absolute values of the Berry curvatures at the K and K' valleys are not the same and have opposite signs. Furthermore, for SL-LuX_2, valley polarization reversal [see Fig. 5(d)] will be achieved when the Lu atoms are magnetized in the opposite direction as shown in Fig. 3(c). At this time, the sign of the Berry curvature at the K and K' valleys remains the same, but the absolute values are exchanged.

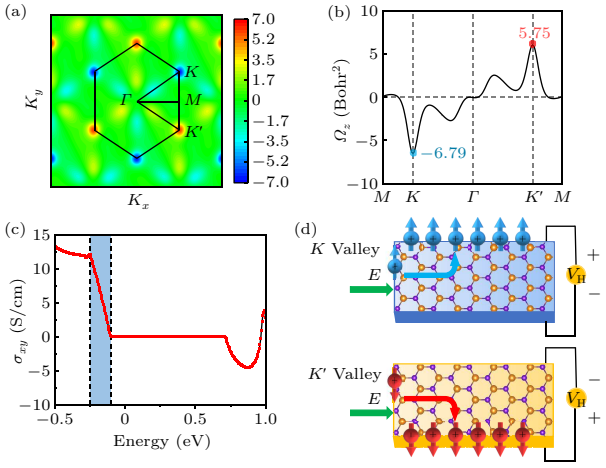


Fig. 5. Berry curvature of SL-LuI_2. (a) and (b) The contour map and the profile along the high symmetry point, respectively, both located in the 2D Brillouin zone. (c) Anomalous Hall conductivity σ_{xy} of SL-LuI_2, the valley extrema are shown by two vertical dashed lines. (d) Schematic illustration of the tunable anomalous valley Hall effect in hole-doped SL-LuX_2, located in the K and K' valleys, respectively. The "+" symbol represents a hole, and spin-up and spin-down are represented by blue arrows and red arrows, respectively.

The considerable spontaneous valley polarization in SL-LuX_2 allows the Fermi level to be located in the light-blue region sandwiched between the two dashed lines of the K valley and the K' valley [see Fig. 5(c)]. This time, a fully spin- and valley-polarized Hall conductivity will be generated, resulting in the net Hall current. Based on the formula

$$\sigma_{xy} = \frac{e^2}{h}\frac{1}{2\pi}\int_{\mathrm{BZ}} \mathrm{d}\boldsymbol{k}^2\Omega(k).$$

The Berry curvature will affect the motion of Bloch electrons under the in-plane electric field, which will acquire an anomalous velocity whose direction is perpendicular to the electric field and whose magnitude is proportional to the Berry curvature, i.e., $v_a \sim E \times \Omega(k)$. Due to the different signs of the

Berry curvature at the K and K' valleys, the charge carriers move in opposite directions, respectively. The charge carriers around the Γ point have almost zero Berry curvature, so they can move along the electric field without lateral motion. Therefore, as the interesting AVHE is realized in SL-LuX_2, as shown in Fig. 4(d), net carriers with the same charge and spin will accumulate on one of its boundaries, forming charge and spin Hall current.

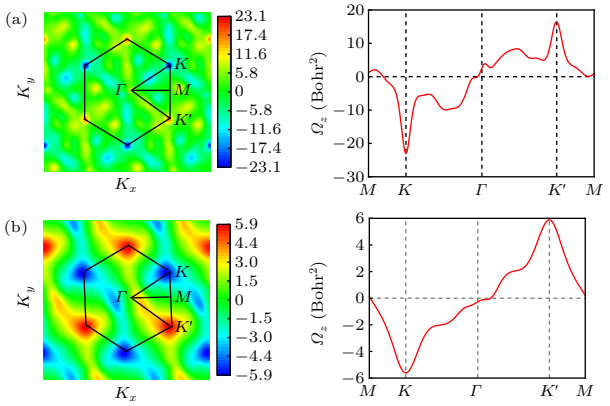


Fig. 6. (a) SL-LuBr$_2$ and (b) SL-LuCl$_2$, contour plots and profiles along high symmetry points of berry curvature.

3.4. Effects of strain on valley splitting

Notably, higher robustness is important for 2D valley-polarized materials. Because it is well known that in actual device fabrication, the 2D material needs to be supported by the substrate, which inevitably introduces strain into the 2D material. Therefore, we applied biaxial in-plane strain to SL-LuI$_2$ to explore the strain effect of SL-LuX_2 through theoretical calculations. The in-plane lattice constants of strained and unstrained SL-LuI$_2$ are represented by a and a_0, respectively, then $\varepsilon = (a - a_0)/a_0 \times 100\%$ can represent the magnitude of the strain. The positive and negative values of ε correspond to tensile and compressive strains, respectively.

As shown in Fig. 7, the value of valley polarization increases monotonically with ε and reaches as high as 173 meV at 5% tensile strain. Interestingly, similar effects were found in other materials with substrates, such as $MoTe_2$ monolayer[49] and $CuCrP_2Te_6$ monolayer.[50] More importantly, even under −5% compressive strain, the valley polarization of SL-LuI$_2$ still reaches an astonishing 115 meV. Therefore, it cannot be denied that the strain of SL-LuI$_2$ has great robustness.

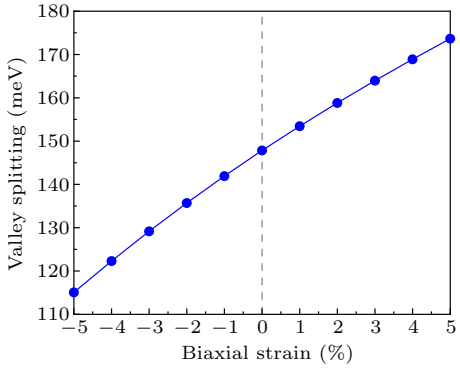


Fig. 7. Valley splitting of SL-LuI$_2$. The in-plane biaxial strain varies from −5% to 5%.

3.5. The U-dependence of the band structures for LuX_2

In general, different U-values will have a significant impact on the band structure. For SL-LuX_2, as shown in Fig. 8, we take SL-LuI$_2$ as an example to calculate the band structure of different U-values after considering SOC. In some previous work, some U values of 4–6 have been applied to the Lu atom.[50–53] In order to better illustrate the dependence of SL-LuX_2 on the U value, we set the range of U values to 1–8.

Interestingly, when the U-value is greater than 4, the K and K' valley on the conduction band will form a ring, respectively. And when the U-value is further increased to 8, the K' valley on the conduction band disappears. However, it is clear that the valley polarization on the valence band is still there. As shown in Fig. 9, as the U-value increases, the band gap E_g and valley splitting increase and decrease monotonically, respectively. And similar U-dependence is reported in $GdCl_2$.[25]

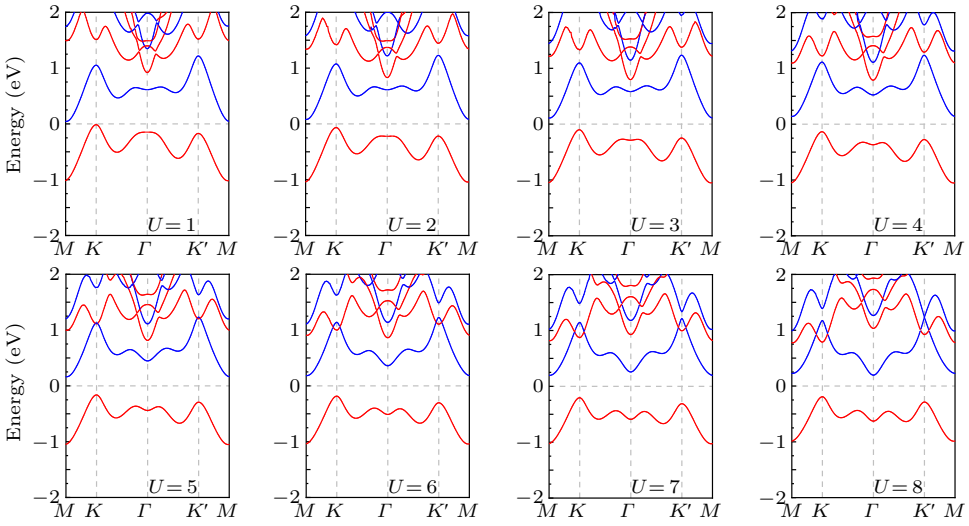


Fig. 8. The band structure of SL-LuI$_2$ when the value of U varies from 1 to 8.

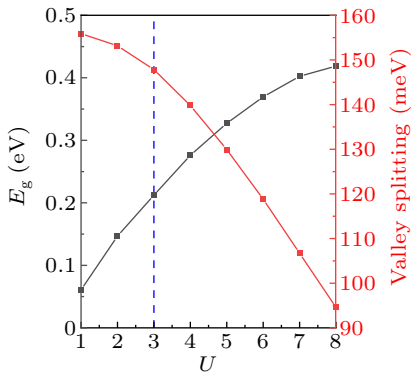


Fig. 9. The band gap E_g and valley splitting vary with U-values.

Even when the U-value is 8, the valley polarization can still be as high as 94.5 meV, indicating that the valley polarization of SL-LuI$_2$ is quite robust.

4. Conclusion

In summary, through first-principles calculations, we reveal that SL-LuX_2 are 2D intrinsic FM materials with huge valley-polarization up to 55 meV–148 meV, which is sufficient for easy memory access and valley polarization regulation. First, it has good thermodynamic stability. Moreover, the Berry curvatures at K and K' have different signs and unequal absolute values, so that SL-LuX_2 provides us with a platform for selectively manipulating valley states and controlling AVHE. In addition, when applying strain of -5% to $+5\%$ to SL-LuI$_2$, the valley polarization response monotonically increases from 115 meV to 173 meV, demonstrating that the valley-polarization of SL-LuX_2 is very robust to strain. Therefore, SL-LuX_2 are very attractive intrinsic ferrovalley materials for experimentation and subsequent applications.

Acknowledgments

Project supported by the Taishan Scholar Program of Shandong Province, China (Grant No. ts20190939), the Independent Cultivation Program of Innovation Team of Jinan City (Grant No. 2021GXRC043), and the National Natural Science Foundation of China (Grant No. 52173283).

References

[1] Zeng H, Dai J, Yao W, Xiao D and Cui X 2012 *Nat. Nanotechnol.* **7** 490
[2] Sun H, Li S S, Ji W X and Zhang C W 2022 *Phys. Rev. B* **105** 195112
[3] Ding J, Qiao Z, Feng W, Yao Y and Niu Q 2011 *Phys. Rev. B* **84** 195444
[4] Mak K F, He K, Shan J and Heinz T F 2012 *Nat. Nanotechnol.* **7** 494
[5] Zhang M H, Zhang C W, Wang P J and Li S S 2018 *Nanoscale* **10** 20226
[6] Peng R, Ma Y, Zhang S, Huang B and Dai Y 2018 *J. Phys. Chem. Lett.* **9** 3612
[7] Ke C, Wu Y, Yang W, Wu Z, Zhang C, Li X and Kang J 2019 *Phys. Rev. B* **100** 195435
[8] Zhang S J, Zhang C W, Zhang S F, Ji W X, Li P, Wang P J, Li S S and Yan S S 2017 *Phys. Rev. B* **96** 205433
[9] Wang Y P, Ji W X, Zhang C W, Li P, Zhang S F, Wang P J, Li S S and Yan S S 2017 *Appl. Phys. Lett.* **110** 213101
[10] Zhou B, Li Z, Wang J, Niu X and Luan C 2019 *Nanoscale* **11** 13567
[11] Aivazian G, Gong Z, Jones A M, Chu R L, Yan J, Mandrus D G, Zhang C, Cobden D, Yao W and Xu X 2015 *Nat. Phys.* **11** 148
[12] Zhang X X, Cao T, Lu Z, Lin Y C, Zhang F, Wang Y, Li Z, Hone J C, Robinson J A, Smirnov D, Louie S G and Heinz T F 2017 *Nat. Nanotechnol.* **12** 883
[13] Tong W Y, Gong S J, Wan X and Duan C G 2016 *Nat. Commun.* **7** 13612
[14] Liu J, Hou W J, Cheng C, Fu H X, Sun J T and Meng S 2017 *J. Phys. Condens. Matter* **29** 255501
[15] Zhao P, Ma Y, Wang H, Huang B, Kou L and Dai Y 2020 arXiv: 2003.04561
[16] Li X, Cao T, Niu Q, Shi J and Feng J 2013 *Proc. Natl. Acad. Sci. USA* **110** 3738
[17] Zhao P, Ma Y, Lei C, Wang H, Huang B and Dai Y 2019 *Appl. Phys. Lett.* **115** 261605
[18] Jiang P, Kang L, Li Y L, Zheng X, Zeng Z and Sanvito S 2021 *Phys. Rev. B* **104** 035430
[19] Cui Q, Zhu Y, Liang J, Cui P and Yang H 2021 *Phys. Rev. B* **103** 085421
[20] Zhao W, Dong B, Guo Z, Su G, Gao R, Wang W and Cao L 2016 *Chem. Commun.* **52** 9228
[21] Coelho P M, Nguyen Cong K, Bonilla M, Kolekar S, Phan M H, Avila J, Asensio M C, Oleynik I I and Batzill M 2019 *J. Phys. Chem. C* **123** 14089
[22] Feng J, Biswas D, Rajan A, *et al.* 2018 *Nano Lett.* **18** 4493
[23] Cheng H X, Zhou J, Ji W, Zhang Y N and Feng Y P 2021 *Phys. Rev. B* **103** 125121
[24] Liu W, Tong J, Deng L, Yang B, Xie G, Qin G, Tian F and Zhang X 2021 *Mater. Today Phys.* **21** 100514
[25] Guo S D, Zhu J X, Mu W Q and Liu B G 2021 *Phys. Rev. B* **104** 224428
[26] Kresse G and Joubert D 1999 *Phys. Rev. B* **59** 1758
[27] Blochl P E 1994 *Phys. Rev. B Condens. Matter* **50** 17953
[28] Kresse G and Furthmüller J 1996 *Phys. Rev. B* **54** 11169
[29] Kresse G and Furthmüller J 1996 *Comput. Mater. Sci.* **6** 15
[30] Perdew J P, Burke K and Ernzerhof M 1998 *Phys. Rev. Lett.* **80** 891
[31] Perdew J P, Burke K and Ernzerhof M 1996 *Phys. Rev. Lett.* **77** 3865
[32] Dudarev S L, Botton G A, Savrasov S Y, Humphreys C J and Sutton A P 1998 *Phys. Rev. B* **57** 1505
[33] Steiner S, Khmelevskyi S, Marsmann M and Kresse G 2016 *Phys. Rev. B* **93** 224425
[34] Togo A and Tanaka I 2015 *Scr. Mater.* **108** 1
[35] Gonze X and Lee C 1997 *Phys. Rev. B* **55** 10355
[36] Bucher D, Pierce L C, McCammon J A and Markwick P R 2011 *J. Chem. Theory Comput.* **7** 890
[37] Nosé S 1984 *Mol Phys.* **52** 255
[38] Nosé S 1984 *J. Chem. Phys.* **81** 511
[39] Mostofi A A, Yates J R, Lee Y S, Souza I, Vanderbilt D and Marzari N 2008 *Computer Phys. Commun.* **178** 685
[40] Huang B, Clark G, Navarro-Moratalla E, Klein DR, Cheng R, Seyler KL, Zhong D, Schmidgall E, McGuire M A, Cobden D H, Yao W, Xiao D, Jarillo-Herrero P, Xu X 2017 *Nature* **546** 270
[41] Gong C, Li L, Li Z, Ji H, Stern A, Xia Y, Cao T, Bao W, Wang C, Wang Y, Qiu Z Q, Cava R J, Louie S G, Xia J and Zhang X 2017 *Nature* **546** 265
[42] Liu L, Ren X, Xie J, Cheng B, Liu W, An T, Qin H and Hu J 2019 *Appl. Surf. Sci.* **480** 300
[43] Mermin N D and Wagner H 1966 *Phys. Rev. Lett.* **17** 1133
[44] Ashton M, Gluhovic D, Sinnott S B, Guo J, Stewart D A and Hennig R G 2017 *Nano Lett.* **17** 5251
[45] Zhuang H L and Hennig R G 2016 *Phys. Rev. B* **93** 054429
[46] Fernandez J F, Ferreira M F and Stankiewicz J 1986 *Phys. Rev. B Condens. Matter* **34** 292
[47] Peng R, Ma Y, Xu X, He Z, Huang B and Dai Y 2020 *Phys. Rev. B* **102** 035412
[48] Liu G B, Xiao D, Yao Y, Xu X and Yao W 2015 *Chem. Soc. Rev.* **44** 2643
[49] Zhang Q, Yang S A, Mi W, Cheng Y and Schwingenschlogl U 2016 *Adv. Mater.* **28** 959
[50] Ma X, Sun L, Liu J, Feng X, Li W, Hu J and Zhao M 2020 *Phys. Status Solidi* **14** 2000008
[51] Oh J, Le M, Nahm H H, *et al.* 2016 *Nat. Commun.* **7** 13146
[52] Song G and Zhang W 2016 *Sci. Rep.* **6** 20133
[53] Zhou S, Lou B, Ma C G and Min Y 2022 *J. Lumin.* **241** 118479